Chem

CellPress

Article

Understanding Thermodynamic and Kinetic Contributions in Expanding the Stability Window of Aqueous Electrolytes

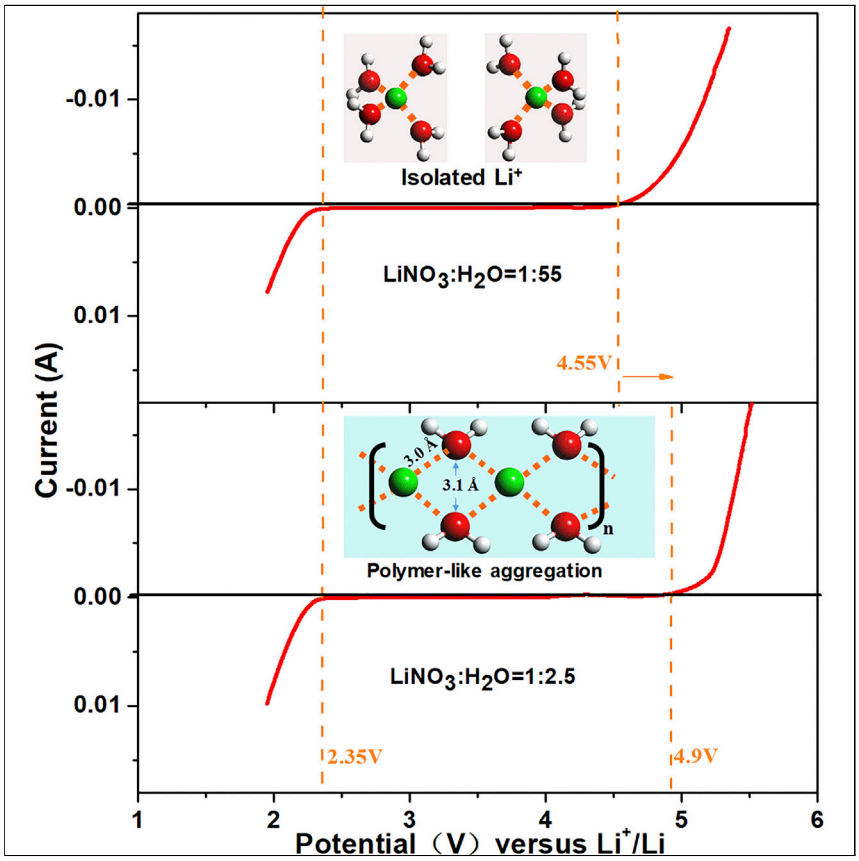

The unique local structure with $(Li^+(H_2O)_2)_n$ polymer-like aggregation in super-concentrated $LiNO_3$ aqueous solution assists in stabilizing the aqueous solution at extreme potentials. Such molecular-level and quantitative understanding will further assist in tailor designing more effective approaches to stabilizing water electrochemically.

Jiaxin Zheng, Guoyu Tan, Peng Shan, ..., Lin-Wang Wang, Kang Xu, Feng Pan

panfeng@pkusz.edu.cn

HIGHLIGHTS

The widened window of a super-concentrated aqueous $LiNO_3$ solution was demonstrated

A local structure of $(Li^+(H_2O)_2)_n$ polymer-like chains was discovered

The local structure is mainly responsible for the expanded electrochemical window

Zheng et al., Chem 4, 2872–2882
December 13, 2018
https://doi.org/10.1016/j.chempr.2018.09.004

Chem

CellPress

Article

Understanding Thermodynamic and Kinetic Contributions in Expanding the Stability Window of Aqueous Electrolytes

Jiaxin Zheng,[1,7] Guoyu Tan,[1,7] Peng Shan,[1,7] Tongchao Liu,[1,7] Jiangtao Hu,[1] Yancong Feng,[1] Luyi Yang,[1] Mingjian Zhang,[1] Zonghai Chen,[2] Yuan Lin,[1] Jun Lu,[2] Joerg C. Neuefeind,[3] Yang Ren,[4] Khalil Amine,[2] Lin-Wang Wang,[5] Kang Xu,[6] and Feng Pan[1,8,*]

SUMMARY

Aqueous electrolytes come with an intrinsic narrow electrochemical stability window (1.23 V). Expanding this window represents significant benefits in both fundamental science and practical battery applications. Recent breakthroughs made via super-concentration have resulted in >3.0 V windows, but fundamental understanding of the related mechanism is still absent. In the present work, we examined the widened window (2.55 V) of a super-concentrated (unsaturated) aqueous solution of $LiNO_3$ through both theoretical and spectral analyses and discovered that a local structure of intimate Li^+-water interaction arises at super-concentration, generating $(Li^+(H_2O)_2)_n$ polymer-like chains to replace the ubiquitous hydrogen bonding between water molecules. Such structure is mainly responsible for the expanded electrochemical stability window. Further theoretical and experimental analyses quantitatively differentiate the contributions to this window, identifying the kinetic factor (desolvation) as the main contributor. Such molecular-level and quantitative understanding will further assist in tailor designing more effective approaches to stabilizing water electrochemically.

INTRODUCTION

Aqueous Li-ion batteries (LIBs) are receiving considerable attention[1–6] because of their non-flammable nature, low toxicity, and low production cost. They promise very tempting alternatives to the state-of-the-art LIBs that rely on highly flammable and toxic non-aqueous electrolytes;[7,8] however, their inherently narrow electrochemical stability window (1.23 V) of water sets an upper limit on the practical voltage and energy output. It has been a scientific challenge to eliminate this ultimate restriction by stabilizing water thermodynamically, especially on the anode side where water is reduced to evolve hydrogen. Adjusting pH has been a popular practice in fabricating aqueous energy storage devices, which proved effective in suppressing hydrogen evolution at the anode,[3,9] but this practice is always accompanied by corresponding compromise in stability at the other electrode because the overall electrochemical stability window of aqueous electrolytes remains constant at 1.23 V as governed by a Pourbaix diagram.[2] Kinetic protection presents a more practical alternative through the formation of an interphase on the electrode surface, which is similar to the well-understood solid-electrolyte interphase (SEI) in non-aqueous LIBs, although a dense deposition of protective layer in an aqueous medium has not been deemed possible until recently. The groundbreaking work by Suo et al., followed by Yamada et al., opens a new avenue in this

The Bigger Picture

Because of their non-flammable nature, low toxicity, and low production cost, aqueous Li-ion batteries (LIBs) promise very tempting alternatives to the state-of-the-art LIBs that rely on highly flammable and toxic non-aqueous electrolytes. However, the intrinsic narrow electrochemical stability window (1.23 V) of water sets an upper limit on the practical voltage and energy output. Here, we report a super-concentrated (unsaturated) $LiNO_3$-based aqueous electrolyte that effectively expands the aqueous stability window to 2.55 V. We further revealed that a unique local structure with $(Li^+(H_2O)_2)_n$ polymer-like aggregation arises at the super-concentration, which assists in stabilizing the aqueous solution at extreme potentials via both thermodynamic and kinetic contributions. This fundamental revelation of liquid structure and its effect on the electrochemical stability window provides a new pathway for designing high-voltage aqueous electrolytes.

direction[2,3,6,10–12] with the adoption of a few selected Li salts at extremely high concentrations (>20 M). Electrochemical stability windows of these aqueous electrolytes was expanded to >3.0 V but with the strict confinement to only a few costly Li salts with anions bearing perfluorinated alkyl substituents. The expanded voltage window in these works was attributed to the scarcity of free water molecules as a result of high salt concentration (thermodynamic) and the formation of a protective SEI of anion origin (kinetic), respectively.

Although these pioneering efforts led to unprecedented stabilization of aqueous electrolytes, such improvements were achieved with expensive Li salts such as lithium bis(trifluoromethane sulfonyl)imide (LiTFSI),[2] lithium bis(pentafluoroethane sulfonyl)imide (LiBETI),[6] and lithium trifluoromethane sulfonate (LiOTF),[10] whose adoption in large-scale applications raises questions. On the fundamental level, there was also little understanding about how the individual thermodynamic and kinetic factors contribute to the expanded voltage windows. In particular, these super-concentrated aqueous solutions present completely new realms of solutions, whose local structure should significantly differ from those well established for dilute aqueous solutions,[13] and hence directly dictate the thermodynamic states of water molecules and salt anions and thus their corresponding electrochemical behaviors. Although in a more recent work some of these authors realized the possible existence of unique local structures in those super-concentrated electrolytes,[14] they failed to make a direct correlation to the electrochemical stability, let alone quantitatively differentiate the contributions from thermodynamic and kinetic factors to such new electrochemical properties.

Here, we report a super-concentrated (unsaturated) aqueous electrolyte that is based on a commodity Li salt, $LiNO_3$ and effectively expands the aqueous stability window to 2.55 V without the need to form a protective SEI. Combining theoretical and experimental approaches, we identified a local structure in the solution as the result of a condensed Li^+-hydration sheath, whose self-assembly into linear aggregation between Li^+ and water molecules generates $(Li^+(H_2O)_2)_n$ polymer-like chain. In such polymer-like aggregation, a great number of Li^+ pairs share water molecules, and the hydrogen-bonding network, ubiquitous in neat water or diluted aqueous solutions, was replaced by intimate Li^+-O_H (water oxygen) interactions. Molecular dynamics (MD) simulations and pair-distribution function (PDF) using high-energy X-ray diffraction revealed that the distance between the two water oxygen atoms in the Li^+-O_H chain is only 3.1 Å. Further theoretical calculations combined with calorimetry studies precisely determined the thermodynamic contribution from the chain-like aggregation to be only 0.015–0.029 V, which is far outweighed by the electrochemical measurement (about 0.6–0.7 V). This quantitative differentiation not only sheds light on the hitherto unexplored local structure of super-concentrated aqueous solutions but also provides molecular-level understanding and guidelines to further tailor the electrochemical properties of these electrolyte materials.

RESULTS AND DISCUSSION

Self-Assembled $(Li^+(H_2O)_2)_n$ Polymer-like Chain

From the measured solubility curve of $LiNO_3$, one can find a large increase (from 117 to 163 g) in $LiNO_3$ solubility from 30°C to 35°C, corresponding to a sudden jump in the salt/water molar ratio (Li^+:H_2O) from 1:3.3 to 1:2.35 (Figure S1). The latter number approaches the super-concentrated aqueous electrolytes named either water-in-salt (2.6),[2] water-in-bisalt (2.0),[10] or hydrate melt (2.0).[6] Although the unsaturated or saturated $LiNO_3$ aqueous electrolytes have been previously reported,[1,15–18] they were

[1]School of Advanced Materials, Peking University, Shenzhen Graduate School, Shenzhen 518055, People's Republic of China

[2]Chemical Sciences and Engineering Division, Argonne National Laboratory, Argonne, IL 60439, USA

[3]Spallation Neutron Source, Oak Ridge National Laboratory, Oak Ridge, TN 37831, USA

[4]X-ray Science Division, Argonne National Laboratory, Argonne, IL 60439, USA

[5]Materials Science Division, Lawrence Berkeley National Laboratory, Berkeley, CA 94720, USA

[6]US Army Research Laboratory, Adelphi, MD 20783, USA

[7]These authors contributed equally

[8]Lead Contact

*Correspondence: panfeng@pkusz.edu.cn

https://doi.org/10.1016/j.chempr.2018.09.004

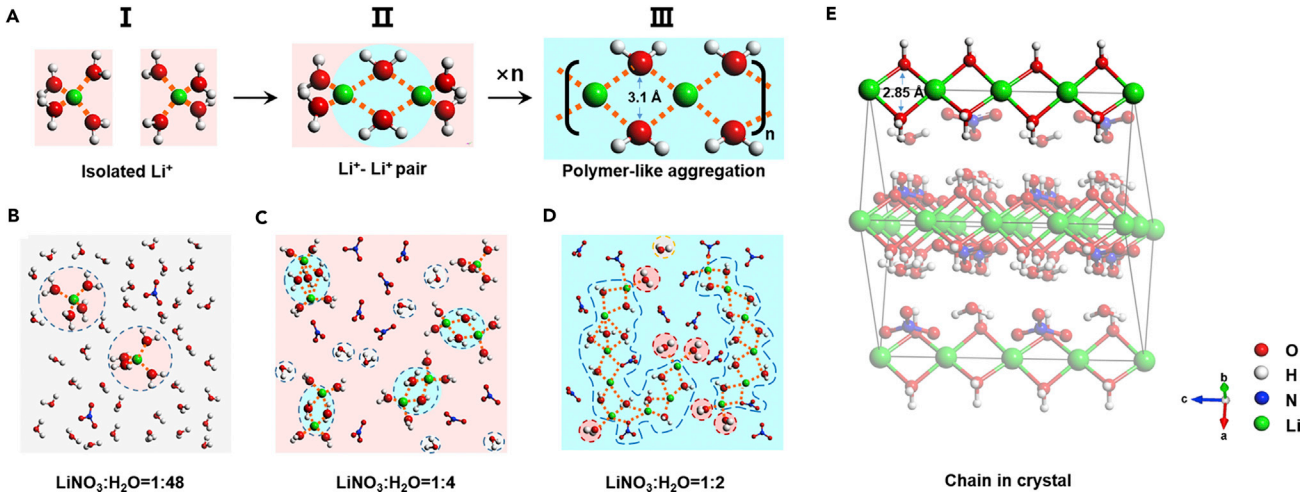

Figure 1. Molecular Dynamics (MD) Simulations of the $LiNO_3$ Aqueous Solution with the Increasing Concentration

(A) Illustration of the evolution of the Li^+ primary solvation sheath from diluted to highly concentrated $LiNO_3$ aqueous solution.

(B–D) MD simulated local structure evolution of $LiNO_3$ aqueous solution from concentration of 1:48 ($LiNO_3$:H_2O) (B) to 1:4 (C) to 1:2 (D).

(E) Crystal structure of $LiNO_3 \cdot 3H_2O$ and the $(Li^+(H_2O)_2)_n$ polymer-like chains in the crystal.

prepared at room temperature and did not reach the super-concentrated state like the reported water-in-salt electrolytes. Thus, the $LiNO_3/H_2O$ system at 35°C was chosen because of the high ionic population of $LiNO_3$ in water and its simple chemical structure containing only three elements, which makes both the theoretical and experimental study of its solution structure much easier than with the polyatomic TFSI and BETI structures. All the simulations and experiments were also conducted at 35°C in the following text. On the basis of the well-developed force fields both for NO_3^-[19–26] and water systems H_2O,[27–31] here we first used MD simulations to depict the structure evolution for $LiNO_3$ aqueous solution with increasing concentration. In classic aqueous solutions whose salt-to-water (S/W = $LiNO_3/H_2O$) molar ratio falls below 1:10, Li^+ forms a $Li^+(H_2O)_4$ complex and moves with this first solvation sheath composed of four water molecules,[32–34] with each individual Li^+ ion randomly scattered throughout the solution. This picture is exactly what the MD simulation snapshot captures for a $LiNO_3$ solution at 200 ns, wherein S/W = 1:48 (Figures 1A-I and 1B; also see details in Supplemental Information Section S1 and Figure S2), and the individual NO_3^- is dispersed randomly among the water molecules without any coordination. However, even in such extremely dilute solution, Li^+ distribution still possesses certain short-range regularity. The first Li^+–Li^+ peak is located at 4.5 Å, as shown in the radial distribution functions (Figure S3), and a small amount of Li^+ pairs can be found in the image of dilute solution, where two Li^+ ions simultaneously coordinate with two to three water molecules to generate $Li_2^+(H_2O)_6$ dimer (Figure 1A-II). In this dilute solution, only 1.9% of water molecules are shared by Li^+ pairs, and 16.1% of water molecules are coordinated by isolated Li^+ ions. Most Li^+ ions carry their complete solvation sheaths with at least four water molecules, and 82% of water molecules remain free and interact with each other only via hydrogen bonds.

When the salt concentration increases to S/W = 1:4, the number of free water molecules rapidly drops to 10.6% (Figures 1C and S4); at S/W = 1:2, only 1.2% of water molecules are still free (Figures 1D and S4). By contrast, with increasing salt concentration, more and more Li^+ ions appear in pairs because they tend to partially share the primary water sheaths with each other; thus the number of water molecules shared by Li^+ increases accordingly. This process bears close resemblance to the

condensation reaction of hydroxyl-containing monomers well established in polymer chemistry (Figures 1C and 1D). Furthermore, with S/W between 1:4 and 1:2, an extended linear chain of Li^+ and water molecules forms (Figure 1A-III), where most of the $Li^+(H_2O)_4$ complex condenses into $(Li^+(H_2O)_2)_n$ (Figure 1D), accompanied by complete disappearance of hydrogen bonds. This dynamic picture from MD simulations directly reflects the drastic transformation in local structure from dilution to super-concentration. Interestingly, it is found that $LiNO_3$ can crystallize with three water molecules to form a hydrate lattice $LiNO_3 \cdot 3H_2O$ at room temperature (Figures 1E and S5–S9), which can be precipitated from the super-concentrated $LiNO_3$ aqueous solution (see Supplemental Information Section S2). In this hydrate crystal lattice, $(Li^+(H_2O)_2)_n$ chains are kept intact surrounded by NO_3^- by electrostatic interactions, and can be viewed as the "living fossil" image frozen from the local liquid structure during its precipitation from the super-concentrated solution. However, the distance between two oxygen atoms belonging to the two nearest water molecules ($d(O_H–O_H)$) in Li^+-H_2O chains of the $LiNO_3 \cdot 3H_2O$ crystal structure is 2.85 Å, while it is 3.1 Å in Li^+-H_2O chains in super-concentrated $LiNO_3$ solution (Figure 1A-III). Compared with dilute $LiNO_3$ solution and a $LiNO_3 \cdot 3H_2O$ crystal, the local structure of aggregated $(Li^+(H_2O)_2)_n$ chains adopts a much more relaxed conformation; thus Li^+ ions could still remain mobile in such structures. It represents a unique characteristic for the super-concentrated $LiNO_3$ solution, which situates itself midway between a crystal and a classic solution with merits from both, and is destined to reflect in macroscopic physical and chemical properties.

Experimental Proof for the $(Li^+(H_2O)_2)_n$ Polymer-like Chains

To validate the existence of such $(Li^+(H_2O)_2)_n$ polymer-like chain structure predicted by MD simulations, the atomic PDF analysis using high-energy X-ray diffraction was conducted at beamline 11-ID-C at the Advanced Photon Source with light wavelength of 0.11729 Å for pure water and $LiNO_3$ aqueous solutions with concentrations of S/W = 1:20, 1:5, 1:3, and 1:2.5 at 35°C (Figure 2A). There are three main peaks that represent the distance between the O atom and N atom in NO_3^- ($d(N–O_N)$), the distance between two oxygen atoms in NO_3^- ($d(O_N–O_N)$), and $d(O_H–O_H)$ (Figure 2B), respectively. We can see that when the $LiNO_3$ solutions transition from the dilute to the super-concentration, $d(N–O_N)$ and $d(O_N–O_N)$ remain unchanged, but the $d(O_H–O_H)$ becomes larger. Figure S10 shows the calculated PDF results for $LiNO_3$ aqueous solution in different concentrations. Figures 2C and 2D compare the calculated and experimental PDF results for diluted and super-concentrated $LiNO_3$ aqueous solutions from 1.8 to 8 Å, respectively. It is immediately apparent that a perfect consistency exists between the MD simulations and experiments for both dilute and super-concentrated $LiNO_3$ aqueous solutions. A peak at 2.1 Å that represents the $d(O_N–O_N)$ in NO_3^- is observed in both solutions (Figures 2C and 2D), whereas the peak at 2.8 Å in dilute solution represents the $d(O_H–O_H)$ between two nearest water molecules connected through a hydrogen bond. As the salt concentration increases, this peak shifts upward to 3.1 Å and becomes broader and weaker in intensity, and the two nearest water molecules become coordinated by a common Li^+, resulting in the formation of the $(Li^+(H_2O)_2)_n$ polymer-like chains (Figure 1A-III). During the process, the original hydrogen bond network is completely replaced by Li^+-O_H (water oxygen) interactions. At super-concentrated states, a series of new peaks also appear both in MD simulated and experimental PDFs, the first of which is located at 4.7 Å. According to our MD simulations, it may represent the $d(O_H–O_N)$ between the oxygen of H_2O in $(Li^+(H_2O)_2)_n$ and NO_3^- by electrostatic interactions. We also did a non-elastic neutron PDF test for the super-concentrated $LiNO_3$ aqueous electrolyte (S/W = 1:2.5), as shown in Figure S11. It looks nearly the same as the atomic

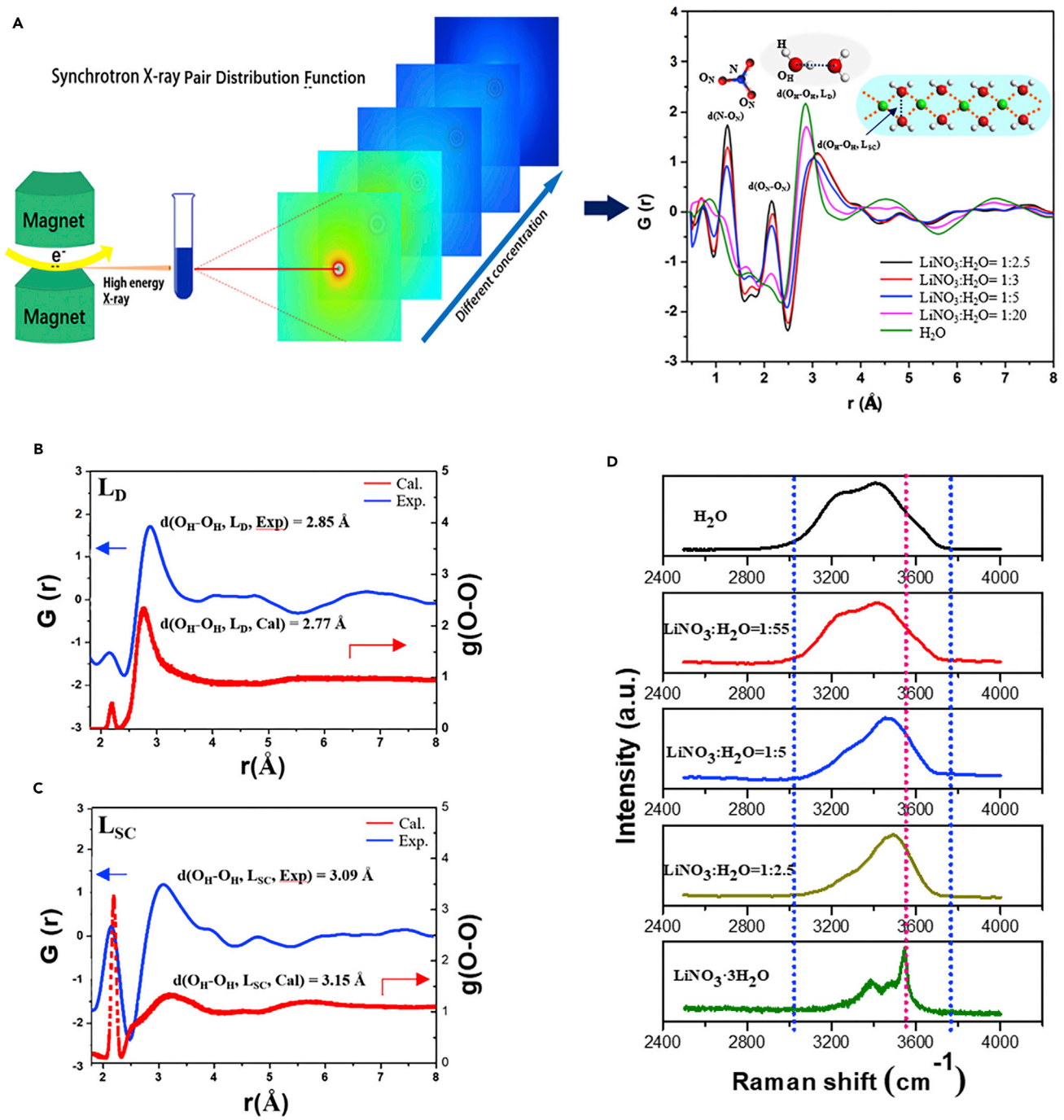

Figure 2. Experimental Proof of the Existence of the $(Li^+(H_2O)_2)_n$ Polymer-like Chains

(A) Schematic illustration of the experimental setup for atomic pair-distribution function (PDF) analysis of high-energy X-ray diffraction.

(B and C) PDF results of pure water and $LiNO_3$ aqueous solution with different concentrations. The comparison of calculated and experimental PDF results for dilute $LiNO_3$ aqueous solution (L_D) (B) and super-concentrated $LiNO_3$ aqueous solution (L_{SC}) (C). d(N-O_N), d(O_N–O_N), and d(O_H–O_H) represent the distance between the O atom and N atom in NO_3^-, the distance between two oxygen atoms in NO_3^-, and the distance between two oxygen atoms belonging to the two nearest water molecules.

(D) Raman spectra of $LiNO_3$ aqueous solution with increasing the salt concentration. Raman spectrum of pure water is also provided for comparison.

PDF analysis using high-energy X-ray diffraction and the MD simulations (Figure 2D), which further validates the existence of the $(Li^+(H_2O)_2)_n$ polymer-like chain structure generated in super-concentrated $LiNO_3$ aqueous electrolyte.

Raman spectroscopy was used to further characterize the O_H–H stretching vibration modes at different Li^+ concentrations (Figure 2E). In pure water, various water molecules with different hydrogen-bonding environments form water molecular clusters, leading to a broad Raman band consisting of several components of the O_H–H stretching vibration. This result indicates that most of the water molecules remain free from coordination with Li^+. As $LiNO_3$ concentration increases, a new peak at 3,487 cm^{-1} appears with simultaneous disappearance of the broad band, indicating the diminishing population of water molecules at such extreme concentrations. As a comparison, the O_H–H stretching vibration modes of water molecules in LiTFSI solution were also characterized at different concentrations (Figure S12). The resultant Raman spectra are consistent with the previous reported results[2,6] and bear striking similarities to the spectra of $LiNO_3$ solutions. Additional evidence comes from the infrared spectroscopy (IR) analysis of $LiNO_3$ solutions, which was carried out in $LiNO_3$ solutions of different concentrations at 35°C (Figure S13A). The wave number of O_H–H stretching vibration is 3,338 cm^{-1} in pure water and 3,350 cm^{-1} in the $LiNO_3$ aqueous solution of S/W = 1: 55. With increasing concentration, the wave number of this stretching increases, and the peak becomes sharper, indicating the gradual phase out of hydrogen bonds throughout the solution. At the super-concentration of S/W = 1:2.5, the wave number is already identical to that of the hydrate crystal $LiNO_3 \cdot 3H_2O$ with a sharp peak at 3,487 cm^{-1} (Figure S13A). In other words, the chemical environment of water molecules in the solution is the same as that in the lattice of $LiNO_3 \cdot 3H_2O$. Similarity can also be found from the aqueous LiTFSI solutions (Figure S13B). The concentration dependence of the chemical shift on $LiNO_3$ concentration as observed in the proton nuclear magnetic resonance reveals the same transformation process (Figure S14), whose upward displacement is induced by the diminishing hydrogen bond and the increase in Li^+-O_H (water oxygen) interactions. According to our previous work,[35] the average binding energy between one water molecule and Li^+ is about 1.0 eV, and the average water-water binding energy is about 0.27 eV per molecule. So the interaction between the water molecule and the Li ion is stronger than the hydrogen bond between the water molecules. Therefore, in super-concentrated aqueous solution, the limited water population will lead to the diminishing hydrogen bond and the increase in Li^+-O_H (water oxygen) interactions.

Expanding the Electrochemical Window

The electrochemical stability windows of the $LiNO_3$ aqueous solutions with S/W = 1:55 and 1:2.5 are demonstrated in Figure 3A, where linear sweep voltammetry was conducted on Pt electrodes using a scan rate of 10 mV s^{-1}. As a comparison, the electrochemical windows of the LiTFSI-based aqueous solutions (1 M and 21 M) are also displayed. A high anodic limit of ~4.90 V versus Li/Li^+ is observed in the $LiNO_3$ aqueous solution at S/W = 1:2.5, whereas at S/W = 55, the value is only 4.55 V. In comparison, the anodic limit of 21 M LiTFSI aqueous solution is 4.80 V, which decreases to 4.50 V in 1 M LiTFSI aqueous solution. These results suggest that the super-concentrated Li^+ aqueous solution using inorganic $LiNO_3$ achieves the same anodic stability against oxidation as the super-concentrated organic LiTFSI aqueous solution, whereas the cathodic limits remain the same for all solutions. Apparently the resistance of water molecules against oxidation is significantly improved as their O_H atoms are occupied by Li^+, as in the case of $LiNO_3$. As previously reported,[6] the cathodic limit remains almost constant on the Pt surface

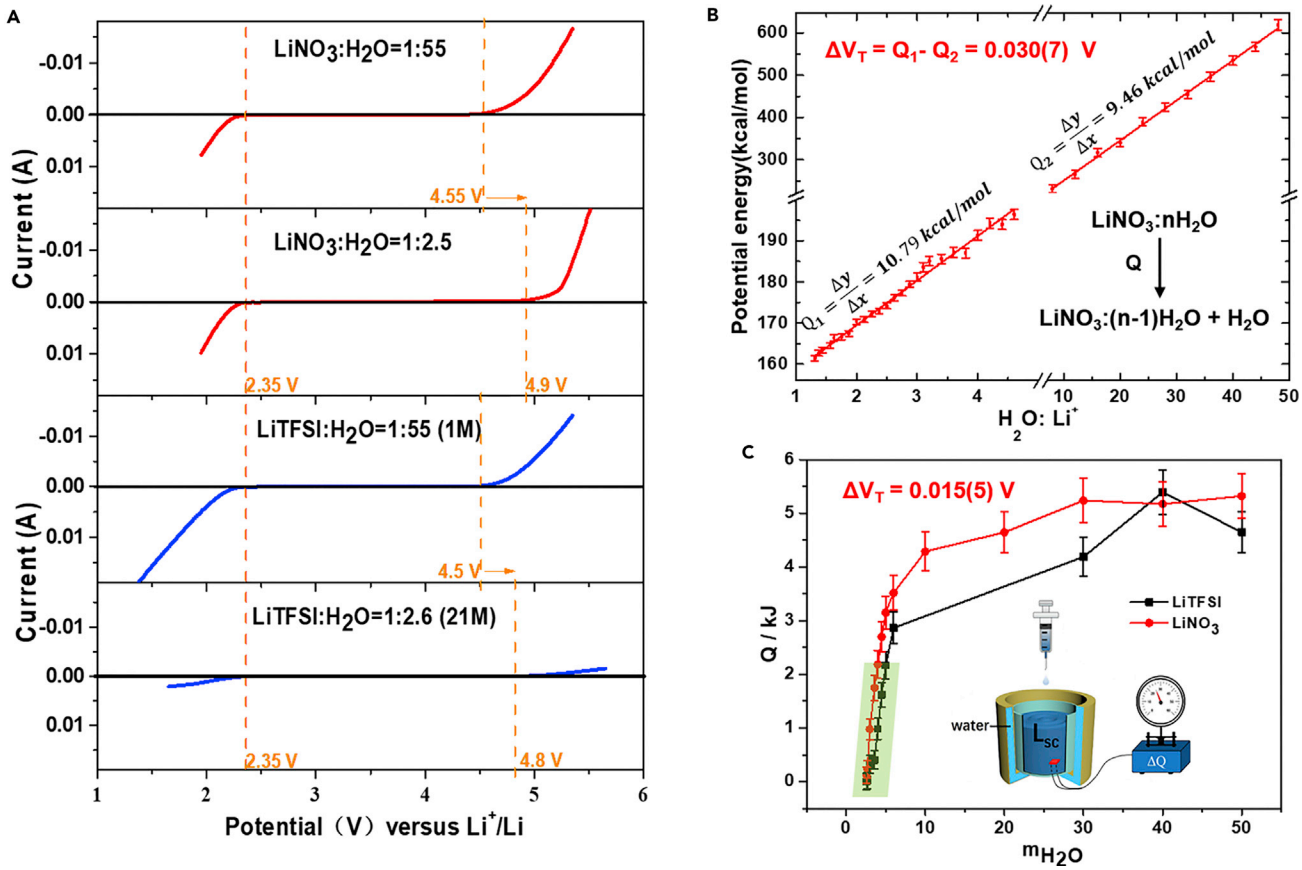

Figure 3. Expanding the Electrochemical Window of Super-Concentrated $LiNO_3$ Aqueous Electrolyte

(A) Potential window of highly concentrated $LiNO_3$ aqueous solution (1:2.5) compared with that of a diluted $LiNO_3$ aqueous solution (1:55) and the typical LiTFSI solutions with concentrations of 21 M and 1 M, evaluated via linear sweep voltammetry (scan rate: 0.1 mVs^{-1}) on Pt electrode.

(B) The MD simulated curve of potential energy versus concentration for $LiNO_3$ solution.

(C) A titration thermal experiment to evaluate the thermodynamic extension: the integrated dilution heat (Q) versus the concentration for the $LiNO_3$ solution (red curve) and LiTFSI solution (black curve).

Error bars correspond to the measurement error of the titration thermal equipment.

(2.35 V), showing no retardation effect on the hydrogen evolution reaction regardless of the salt species or concentrations.

Using MD simulations, we attempted to quantitatively differentiate the contributions to the expanded window (see details in Figure S15 and Supplemental Information Section S2). Figure 3B shows the simulated curve of potential energy versus concentration for $LiNO_3$ solution. We can see that the potential energy shows a linear relationship with the concentration in dilute solution (e.g., from S/W = 1:10 to S/W = 1:50) and highly concentrated solution (e.g., from S/W = 1:2 to S/W = 1:5), respectively. The slope of such energy versus concentration curve indicates the latent heat (Q) of the solution, and the thermodynamic extension can thus be obtained by comparing the difference between the latent heats in diluted and super-concentrated states. Based on this technique, the thermodynamic contribution to the electrochemical stability is estimated to be 0.030(7) V. Thermal titration experiments further verify this quantitative assignment (see more details in Supplemental Information Section S2). The integrated dilution heats (Q) versus the concentration for $LiNO_3$ solution (black curve) and LiTFSI solution (red curve) are shown in Figure 3C. We can clearly see that the Q value displays a nearly linear relationship

with the salt concentration in both diluted (e.g., from S/W = 1:10 to 1:50) and super-concentrated solutions (e.g., from S/W = 1:2.5 to 1:6) both for $LiNO_3$ and for LiTFSI aqueous solutions, in good agreement with the MD simulated results (Figure 3B). Thus, the thermodynamic extension is estimated to be 0.015(5) V both for super-concentrated $LiNO_3$ and LiTFSI aqueous solutions, close to what MD predicts. Despite the minute difference in values, all the preceding results converge into a single conclusion that the thermodynamic stability of the aqueous electrolytes, as induced by the unique local structure consisting of chain-like aggregation, can indeed be improved by the super-concentration of $LiNO_3$, but this contribution is almost negligible (only about 0.01–0.02 V) compared with the overall stabilization as observed by electrochemical measurement (about 0.6–0.7 V). Kinetic factors therefore should have played the major role.

Previous works have attributed the stabilization of aqueous electrolytes to the kinetics protection provided by an interphase formed from reduction of anions (TFSI or BETI) on anode.[2,3,6,10–12] In our aqueous system based on $LiNO_3$, an interphase is not expected, because chemically, $LiNO_3$ cannot provide any building block that can deposit in dense form from aqueous media. Thus, the kinetic contribution should come only from the unique local structure consisting of intimately connected $(Li^+(H_2O)_2)_n$ polymer-like chains. For example, because all the charge-transfer process must occur at the electrode surface, if the journey of a single water molecule is visualized during its decomposition, its first step has to be exit from the bulk solution (desolvation), where it either exists in a cluster (in diluted solution) or in $(Li^+(H_2O)_2)_n$ polymer-like aggregation (in super-concentrated solution), followed by adsorption on the electrode surface. Thus, the different local structure of the single water molecule in diluted solution and super-concentrated solution will lead to the difference in the kinetic barriers in the desolvation process. We can hence attribute the improvements in electrochemical properties mainly to the kinetic contribution, which originates from the unique local structure of intimately connected water and Li^+ in the $(Li^+(H_2O)_2)_n$ polymer-like aggregation.

Performance of Aqueous Super-Concentrated $LiNO_3$ versus LiTFSI Electrolyte Solution for LIBs

A three-electrode electrochemical cell was constructed to evaluate the viability of the super-concentrated $LiNO_3$ solution, where two types of commercial cathode materials, $LiMn_2O_4$ (LMO) and $LiNi_{1/3}Mn_{1/3}Co_{1/3}O_2$ (NMC333), served as working electrodes, and active carbon and Ag/AgCl (in saturated KCl aqueous solution) were used as counter and reference electrodes, respectively. In comparison, the same tests were also conducted with super-concentrated LiTFSI aqueous solution (21 M) as electrolyte. Figure S16 shows the cyclic voltammeter curves of LMO and NMC333 electrodes in aqueous electrolytes with different salt concentrations. We can see that the reversibility is improved significantly in super-concentrated aqueous electrolytes. Figures 4A and 4C show the charge-discharge curves of the aqueous LIB using 1:2.5 $LiNO_3$ electrolyte. At a C rate of 1 C (1 C = 148 and 180 mAh g^{-1}), LMO and NMC333 batteries show discharge capacities of 135 mAh g^{-1} and 165 mAh g^{-1}, respectively. Compared with the charge-discharge curves of diluted (S/W = 1:55) $LiNO_3$ aqueous LIBs (Figure S17), the average discharge voltage is improved by about 0.3 V with super-concentrated $LiNO_3$ (S/W = 1:2.5). Figures 4B and 4D compare the rate capabilities of aqueous LIB cells using both 1:2.5 $LiNO_3$ and 21 M LiTFSI solutions, where no evident difference can be found between them. At current densities of 3 C, 5 C, 10 C, and 20 C, reversible capacities of 120/120, 86/92, 60/63, and 40/38 mAh g^{-1} are achieved for LMO/NMC333 in

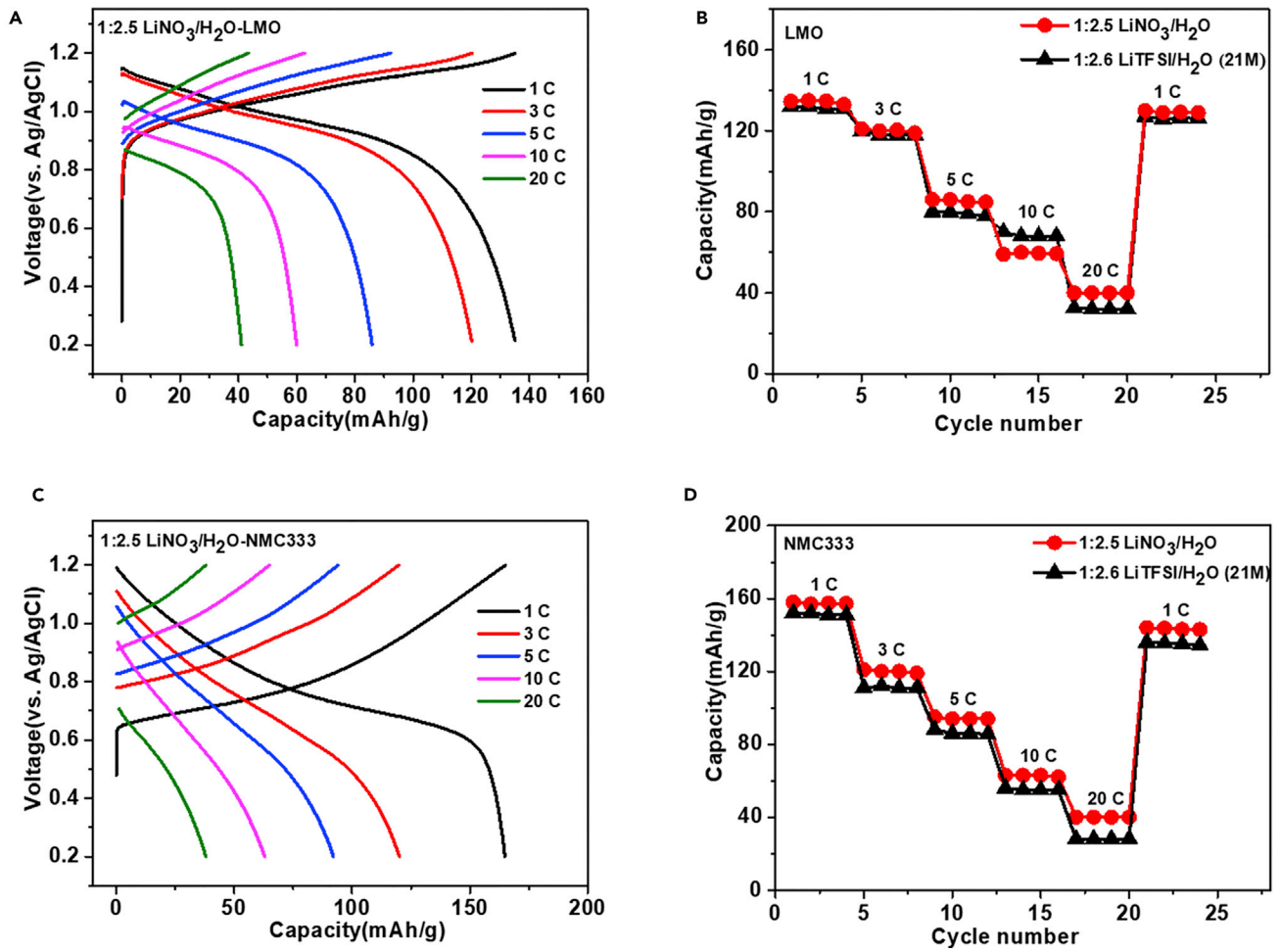

Figure 4. Electrochemical Performance of the Highly Concentrated $LiNO_3$ LIBs

(A and C) The charge–discharge curves of 1:2.5 $LiNO_3$ aqueous electrolyte-based $LiMn_2O_4$ (LMO) (A) and $LiNi_{1/3}Mn_{1/3}Co_{1/3}O_2$ (NMC333) (C) LIBs. (B and D) The rate capability of LMO (B) and NMC333 (C) in the 1:2.5 $LiNO_3$ aqueous solution and the 21 M LiTFSI aqueous solution between 0 and 1.2 V (versus Ag/AgCl), respectively.

1:2.5 $LiNO_3$ aqueous electrolyte, respectively. In addition, 96% of the initial capacity can be retained after 20 cycles. We also chose a high-voltage $LiCoO_2$ material as cathode and cycled it in 1 M (Li^+:H_2O = 1:55) and super-concentrated (Li^+:H_2O = 1:2.5) $LiNO_3$ aqueous electrolytes, respectively. Figure S18 shows their charge and discharge curves. We can see that in dilute $LiNO_3$ aqueous electrolyte (1 M), the water became split seriously during the charge process, and $LiCoO_2$ could not be discharged after charging. By contrast, a $LiCoO_2$ cathode can be cycled reversibly at the voltage of 1.3 V in super-concentrated (Li+:H_2O = 1:2.5) $LiNO_3$ aqueous electrolyte.

Conclusions

In summary, a super-concentrated aqueous electrolyte based on $LiNO_3$ was discovered. It provides an expanded electrochemical stability window of 2.55 V at much lower cost than its counterparts based on LiTFSI, LiBETI, and LiOTF. Extensive MD simulations combined with advanced spectral analysis, including atomic PDF of high-energy X-ray diffraction data, reveal that a unique local structure arises at the super-concentration of $LiNO_3$ in water, where the limited water population

forces the Li^+ to merge their primary solvation sheath, resulting in $(Li^+(H_2O)_2)_n$ polymer-like aggregation. Such a new liquid structure assists in stabilizing the aqueous solution at extreme potentials via both thermodynamic and kinetic contributions. Detailed MD calculations and calorimetry studies further differentiated these contributions quantitatively, and identified the kinetic factor, i.e., the energy barrier for water molecules to free themselves from the $(Li^+(H_2O)_2)_n$ polymer-like aggregation, that dominates the electrochemical stability improvements. This fundamental revelation of liquid structure and its effect on the electrochemical stability window provides a new pathway for the design of high-voltage aqueous electrolytes, where costly Li salts with highly fluorinated anions may no longer be necessary.

EXPERIMENTAL PROCEDURES

Full experimental details are provided in the Supplemental Information.

SUPPLEMENTAL INFORMATION

Supplemental Information includes Supplemental Experimental Procedures (method details, more detailed results of the molecular dynamics, characterization of supersaturated $LiNO_3$ aqueous solution, the thermodynamic extension calculation, the titration experiment that measured the heat of solution, and other experimental results), 18 figures, 2 tables, and 1 data file and can be found with this article online at https://doi.org/10.1016/j.chempr.2018.09.004.

ACKNOWLEDGMENTS

This work was financially supported by the National Materials Genome Project (2016YFB0700600), the National Natural Science Foundation of China (21603007 and 51672012), and Shenzhen Science and Technology Research Grants (JCYJ20150729111733470 and JCYJ20151015162256516). L.-W.W. was supported by the Assistant Secretary for Energy Efficiency and Renewal Energy under the Battery Material Research program. J.L., Z.C., and K.A. gratefully acknowledge support from the Vehicle Technologies Office of the US Department of Energy (DOE) Office of Energy Efficiency and Renewable Energy. Argonne National Laboratory is operated for the DOE Office of Science by UChicago Argonne LLC under contract no. DE-AC02-06CH11357. This research used resources of the Advanced Photon Source, a DOE Office of Science User Facility operated for the DOE Office of Science by Argonne National Laboratory under contract no. DE-AC02-06CH11357. The neutron scattering experiments were carried out at the Spallation Neutron Source, which is sponsored by the Scientific User Facilities Division of the DOE Office of Basic Energy Sciences under contract no. DE-AC05-00OR22725 with the Oak Ridge National Laboratory.

AUTHOR CONTRIBUTIONS

F.P. and J.Z. planned the project and supervised all aspects of the research. J.Z. contributed to writing the manuscript. G.T. and Y.F. performed MD simulations and *ab initio* calculations. P.S. and J.H. performed electrochemical tests. T.L., J.C.N., and Y.R. performed PDF measurements. M.Z. performed single-crystal X-ray diffraction. Y.L. performed the titration experiment to measure the heat of solution. J.Z., G.T., Z.C., J.L., Y.R., K.A., L.-W.W., and F.P. analyzed the data. J.Z. and G.T. drafted the paper, and all authors revised it.

DECLARATION OF INTERESTS

The authors declare no competing financial interests.

Received: April 25, 2018
Revised: July 31, 2018
Accepted: September 13, 2018
Published: October 11, 2018

REFERENCES AND NOTES

1. Li, W., Dahn, J.R., and Wainwright, D.S. (1994). Rechargeable lithium batteries with aqueous electrolytes. Science *264*, 1115–1117.

2. Suo, L., Borodin, O., Gao, T., Olguin, M., Ho, J., Fan, X., Luo, C., Wang, C., and Xu, K. (2015). "Water-in-salt" electrolyte enables high-voltage aqueous lithium-ion chemistries. Science *350*, 938–943.

3. Luo, J.-Y., Cui, W.-J., He, P., and Xia, Y.-Y. (2010). Raising the cycling stability of aqueous lithium-ion batteries by eliminating oxygen in the electrolyte. Nat. Chem. *2*, 760–765.

4. Pasta, M., Wessells, C.D., Huggins, R.A., and Cui, Y. (2012). A high-rate and long cycle life aqueous electrolyte battery for grid-scale energy storage. Nat. Commun. *3*, 1149.

5. Kim, H., Hong, J., Park, K.-Y., Kim, H., Kim, S.-W., and Kang, K. (2014). Aqueous rechargeable Li and Na ion batteries. Chem. Rev. *114*, 11788–11827.

6. Yamada, Y., Usui, K., Sodeyama, K., Ko, S., Tateyama, Y., and Yamada, A. (2016). Hydrate-melt electrolytes for high-energy-density aqueous batteries. Nat. Energy *1*, 16129.

7. Hu, L., and Xu, K. (2014). Nonflammable electrolyte enhances battery safety. Proc. Natl. Acad. Sci. U S A *111*, 3205–3206.

8. Hammami, A., Raymond, N., and Armand, M. (2003). Lithium-ion batteries: runaway risk of forming toxic compounds. Nature *424*, 635–636.

9. Li, W., McKinnon, W.R., and Dahn, J.R. (1994). Lithium intercalation from aqueous solutions. J. Electrochem. Soc. *141*, 2310–2316.

10. Suo, L., Borodin, O., Sun, W., Fan, X., Yang, C., Wang, F., Gao, T., Ma, Z., Schroeder, M., and von Cresce, A. (2016). Advanced high-voltage aqueous lithium-ion battery enabled by "water-in-bisalt" electrolyte. Angew. Chem. Int. Ed. *55*, 7136–7141.

11. Suo, L., Borodin, O., Wang, Y., Rong, X., Sun, W., Fan, X., Xu, S., Schroeder, M.A., Cresce, A.V., and Wang, F. (2017). "Water-in-salt" electrolyte makes aqueous sodium-ion battery safe, green, and long-lasting. Adv. Energy Mater *7*, 1701189.

12. Yang, C., Chen, J., Qing, T., Fan, X., Sun, W., von Cresce, A., Ding, M.S., Borodin, O., Vatamanu, J., Schroeder, M.A., et al. (2017). 4.0 V aqueous Li-ion batteries. Joule *1*, 122–132.

13. Brini, E., Fennell, C.J., Fernandez-Serra, M., Hribar-Lee, B., Lukšič, M., and Dill, K.A. (2017). How water's properties are encoded in its molecular structure and energies. Chem. Rev. *117*, 12385–12414.

14. Borodin, O., Suo, L., Gobet, M., Ren, X., Wang, F., Faraone, A., Peng, J., Olguin, M., Schroeder, M., Ding, M.S., et al. (2017). Liquid structure with nano-heterogeneity promotes cationic transport in concentrated electrolytes. ACS Nano *11*, 10462–10471.

15. Li, N., Patrissi, C.J., Che, G., and Martin, C.R. (2000). Rate capabilities of nanostructured $LiMn_2O_4$ electrodes in aqueous electrolyte. J. Electrochem. Soc. *147*, 2044–2049.

16. Liu, J., Yi, L., Liu, L., and Peng, P. (2015). LiV_3O_8 nanowires with excellent stability for aqueous rechargeable lithium batteries. Mater. Chem. Phys. *161*, 211–218.

17. Zhao, M., Zhang, W., Qu, F., Wang, F., and Song, X. (2014). Good discharge capacities of NaV_6O_{15} material for an aqueous rechargeable lithium battery. Electrochim. Acta *138*, 187–192.

18. Zhao, M., Zheng, Q., Wang, F., Dai, W., and Song, X. (2011). Electrochemical performance of high specific capacity of lithium-ion cell LiV_3O_8//$LiMn_2O_4$ with $LiNO_3$ aqueous solution electrolyte. Electrochim. Acta *56*, 3781–3784.

19. Jensen, K.P., and Jorgensen, W.L. (2006). Halide, ammonium, and alkali metal ion parameters for modeling aqueous solutions. J. Chem. Theor. Comput. *2*, 1499–1509.

20. Jorgensen, W.L., Maxwell, D.S., and Tirado-Rives, J. (1996). Development and testing of the OPLS all-atom force field on conformational energetics and properties of organic liquids. J. Am. Chem. Soc. *118*, 11225–11236.

21. Jorgensen, W.L., and Tirado-Rives, J. (2005). Potential energy functions for atomic-level simulations of water and organic and biomolecular systems. Proc. Natl. Acad. Sci. U S A *102*, 6665–6670.

22. Kaminski, G.A., Friesner, R.A., Tirado-Rives, J., and Jorgensen, W.L. (2001). Evaluation and reparametrization of the OPLS-AA force field for proteins via comparison with accurate quantum chemical calculations on peptides. J. Phys. Chem. B *105*, 6474–6487.

23. McDonald, N.A., and Jorgensen, W.L. (1998). Development of an all-atom force field for heterocycles. Properties of liquid pyrrole, furan, diazoles, and oxazoles. J. Phys. Chem. B *102*, 8049–8059.

24. Price, M.L., Ostrovsky, D., and Jorgensen, W.L. (2001). Gas-phase and liquid-state properties of esters, nitriles, and nitro compounds with the OPLS-AA force field. J. Comput. Chem. *22*, 1340–1352.

25. Rizzo, R.C., and Jorgensen, W.L. (1999). OPLS all-atom model for amines: resolution of the amine hydration problem. J. Am. Chem. Soc. *121*, 4827–4836.

26. Watkins, E.K., and Jorgensen, W.L. (2001). Perfluoroalkanes: conformational analysis and liquid-state properties from ab initio and Monte Carlo calculations. J. Phys. Chem. A *105*, 4118–4125.

27. Berendsen, H.J., Postma, J.P., van Gunsteren, W.F., and Hermans, J. (1981). Interaction models for water in relation to protein hydration. In Intermolecular Forces, B. Pullman, ed. (Springer), pp. 331–342.

28. Jorgensen, W.L. (1981). Quantum and statistical mechanical studies of liquids. 10. transferable intermolecular potential functions for water, alcohols, and ethers. Application to liquid water. J. Am. Chem. Soc. *103*, 335–340.

29. Jorgensen, W.L., Chandrasekhar, J., Madura, J.D., Impey, R.W., and Klein, M.L. (1983). Comparison of simple potential functions for simulating liquid water. J. Chem. Phys. *79*, 926–935.

30. MacKerell, A.D., Jr., Bashford, D., Bellott, M., Dunbrack, R.L., Jr., Evanseck, J.D., Field, M.J., Fischer, S., Gao, J., Guo, H., and Ha, S. (1998). All-atom empirical potential for molecular modeling and dynamics studies of proteins. J. Phys. Chem. B *102*, 3586–3616.

31. Berendsen, H., Grigera, J., and Straatsma, T. (1987). The missing term in effective pair potentials. J. Phys. Chem. *91*, 6269–6271.

32. Rudolph, W., Brooker, M.H., and Pye, C.C. (1995). Hydration of lithium ion in aqueous solutions. J. Phys. Chem. *99*, 3793–3797.

33. Pye, C.C., Rudolph, W., and Poirier, R.A. (1996). An ab initio investigation of Lithium ion hydration. J. Phys. Chem. *100*, 601–605.

34. Mähler, J., and Persson, I. (2011). A study of the hydration of the alkali metal ions in aqueous solution. Inorg. Chem. *51*, 425–438.

35. Zheng, J., Hou, Y., Duan, Y., Song, X., Wei, Y., Liu, T., Hu, J., Guo, H., Zhuo, Z., and Liu, L. (2015). Janus solid–liquid interface enabling ultrahigh charging and discharging rate for advanced lithium-ion batteries. Nano Lett. *15*, 6102–6109.